Cellular Physiology and Biochemistry

Cell Physiol Biochem 2022;56:484-499
DOI: 10.33594/000000571
Published online: 21 September 2022
Accepted: 1 September 2022

Original Paper

Adenosine Triphosphate Protects from Elevated Extracellular Calcium-Induced Damage in Human Proximal Kidney Cells: Using Deep Learning to Predict Cytotoxicity

Rawad Hodeify[a] Arfan Ghani[b] Rachel Matar[a] Cijo George Vazhappilly[a] Maxime Merheb[a] Hussain Al Zouabi[a] John Marton[a]

[a]Department of Biotechnology, School of Arts and Sciences, American University of Ras Al Khaimah, Ras Al Khaimah, United Arab Emirates, [b]Department of Computer Science and Engineering, School of Engineering, American University of Ras Al Khaimah, Ras Al Khaimah, United Arab Emirates

Key Words
Extracellular calcium • ATP • Calcium-binding proteins • Intracellular calcium • Convolutional neural network (CNN) • Image classification

Abstract
Background/Aims: In kidney, extracellular [Ca^{2+}] can modulate intracellular [Ca^{2+}] to control key cellular processes. Hence, extracellular [Ca^{2+}] is normally maintained within narrow range. We tested effect of extracellular ATP on viability of human proximal (HK-2) cells at high calcium. Modulation of intracellular calcium was assessed by imaging cytosolic [Ca^{2+}], and expression of calcium-binding proteins (CaBPs). We present an artificial intelligence enabled deep learning model for prediction of injury and protection against extracellular [Ca^{2+}] in HK-2 cells. ***Methods:*** HK-2 cells were cultured in calcium-free DMEM supplemented with CaCl2. Morphological changes were detected using light microscopy. Cell viability was determined using MTT Assay. Intracellular [Ca^{2+}] was detected using fluorescence microscopy. For easy detection of HK-2 cells injury, we performed light microscopy image classification based on Convolutional Neural Network. Expression of CaBPs, p21, and Mcl-1 was measured using real-time PCR. ***Results:*** We show decreased viability of HK-2 cells cultured in elevated calcium levels, which was prevented by adenosine triphosphate (ATP). Exposure of cells to elevated extracellular [Ca^{2+}] correlated with increasing fluorescence of intracellular calcium indicator, which was attenuated in presence of ATP. Since features cannot be detected easily by human eyes, we propose a customized deep learning-based CNN model for classification of HK-2 cells injury by extracellular calcium with high accuracy of 98%. Our data demonstrated significant increase in mRNA levels of calmodulin, S100A8, S100A14 and CaBP28k, with elevated

Rawad Hodeify
Assistant Professor of
Medical Biotechnology

Department of Biotechnology, American University of Ras Al Khaimah,
Sheikh Humaid Bin Mohamed Street, Building: 75, Seih Al Araibi, Ras Al Khaimah, 72603 (UAE)
Tel. +971-7-246-8843, Fax +971 7 2210300, E-Mail rawad.hodeify@aurak.ac.ae

extracellular [Ca^{2+}]. Expression of these genes was enhanced with ATP. ***Conclusion:*** The results suggest that ATP protects human proximal (HK-2) cells against elevated extracellular calcium levels. We present a CNN model as user friendly tool to study calcium dependent injury in (HK-2) cells. Finally, we show that ATP-mediated protection is correlated with enhanced expression of calcium-binding proteins.

Introduction

Calcium ion [Ca^{2+}] mediates essential physiological functions through its extracellular and intracellular signaling activities [1, 2]. Tubular fluid supersaturation with respect to calcium and phosphate contribute to the formation of calcium stones in intratubular and/or interstitial regions of nephron [3]. This mechanism increases risk of urine-stone formation and renal damage. Serum calcium elevation has been also detected with reported cases of kidney stone formation [4]. In addition, elevated levels of ionized serum [Ca^{2+}] have been associated with impairment in renal function, reduced glomerular filtration, and acute kidney injury [5-7].

Proximal tubule is a major site for Ca^{2+} reabsorption by the kidney [8, 9]. Proximal tubule cells express calcium sensitive receptor that behaves as a sensor of extracellular ions and its activation by the increase in tubular fluid calcium may protect against calcium-phosphate precipitation [10]. Proximal tubular cells have higher affinity and internalization of calcium crystals than distal tubular cells [11, 12]. Gombedza et al. demonstrated that calcium crystal internalization into human proximal kidney cells activated store-operated Ca^{2+} entry resulting in a sustained rise in intracellular calcium, ER stress response, reactive oxygen species production, and subsequently, cell death [13]. Other studies reported that calcium kidney stone disease is associated directly or indirectly with disruption of mitochondrial activity [14-16]. Besides energy production, mitochondria are also implicated in regulation of intracellular calcium by its uptake from cytosol [17]. Additional mechanisms for maintaining intracellular calcium homeostasis include regulation of Ca^{2+} flowing into and out of the cell, calcium release and uptake to organelles, and modulation of calcium-binding proteins [18].

Apart from the studies demonstrating association of calcium crystals with mitochondrial dysregulation, increased intracellular $[Ca^{2+}]_i$, and proximal cell damage, the potential effect of extracellular adenosine triphosphate (ATP) on survival of HK-2 exposed to high amounts of extracellular calcium have not been studied yet. In this study, we show that extracellular ATP enhances the survival of HK-2 cells cultured in high extracellular calcium and modulated the expression of calcium binding proteins. We also introduced a supervised deep learning approach through convolutional neural network (CNN) model for an easy detection of human proximal HK-2 cells injury by high amounts of extracellular calcium with high accuracy. The performance of our model is remarkably high as reflected in its high accuracy in classification of cells cultured in normal calcium, high calcium, as well as cells incubated in high calcium in the presence of ATP, in a relatively small set of data. We believe that our model offers a unique solution and a user friendly tool for researchers commonly using HK-2 cells *in vitro* models of calcium dependent injury.

Materials and Methods

Materials

Dulbecco's Modified Eagle Medium (DMEM), DMEM calcium-free media, ATP, and Fluo-4 AM were purchased from Gibco/Thermofisher (Waltham, MA, USA). CyQUANT™ MTT Cell Proliferation Assay Kit was ordered from Invitrogen (St. Louis, MO, USA). Glass-bottomed culture dishes for imaging from MatTek (Ashland, MA). Real-time PCR primers were ordered from Gene Link (NY, USA), cDNA synthesis and real-time PCR kits were from Solis BioDyne (Tartu, Estonia).

Cell culture and treatment

Human proximal kidney (HK-2) cells obtained from Applied Biological Materials Inc, Canada, were maintained in Dulbecco's Modified Eagle Medium (Gibco/ Thermofisher) with high glucose (4.5 g/L) supplemented with 10% FBS, 2 mM L-glutamine, and 1 % penicillin-streptomycin at 37°C with 5% carbon dioxide. The standard DMEM media contains 1.8 mM calcium as reported in the company datasheet. Adjusting the required calcium concentration was done in calcium-free media from the same company by adding CaCl2. Cells were seeded overnight and left to reach ~ 60-70% confluency before treatments. The next day, media was removed and replaced either by standard media or calcium-free supplemented with CaCl2 to the required concentration, and the cells were grown for an additional 18-20 h before processing. ATP was added to the media to a final concentration of 50 μM.

MTT Cell Proliferation Assay

Cell proliferation was determined by CyQUANT™ MTT Cell Proliferation Assay Kit (Invitrogen V13154, St. Louis, MO, USA) following the manufacturer's protocol. Briefly, the cells were plated in a 96-well plate at 10,000 cells per well. After overnight attachment, cells were treated with standard media or calcium-free media adjusted with CaCl2, in the presence or absence of ATP, for 18-20 hours. After treatment, the media was removed and replaced with fresh media before adding 10 μl of the MTT drug reconstituted with PBS to each well. Following incubation at 37°C for 4 h, media was removed leaving around 25 μL in the wells, and 100 μl of DMSO was added to each well followed by pipetting up and down to mix thoroughly. The plate was incubated at 37°C for ~10 min to dissolve the insoluble formazan crystals. Absorbance at 490 nm was recorded using Biotek ELx800 microplate reader (Ontario, Canada). Cell viability was quantified based on the absorbance ratio between treated and control conditions.

Light and Fluorescence Microscopy

Light microscopy imaging was done with an inverted OPTIKA XDS-2 microscope (Optika, Italy) with 10X objective. For fluorescent imaging, cells were plated on poly-D-lysine coated glass-bottomed plates (MatTek Corporation) to reach 50-60% confluency before treatment. Fluo-4 AM, a cell-permeant fluorescent calcium indicator (ThermoFischer Scientific, Waltham, MA, USA), was used to detect intracellular calcium. Fluo-4 AM was dissolved in DMSO containing 1% pluronic acid. After treatments, the cells were washed in Hanks' balanced salt solution (HBSS) and loaded with 5 μM Fluo-4 AM for 1 hour in the dark at 37°C. Cells were washed in HBSS, and then incubated in the same buffer for another 20 min before imaging by Optika XDS-2 inverted microscope with M-795 fluorescence system (Optika, Italy) using a green filter. Nuclear staining was done on cells fixed in 4 % paraformaldehyde (PFA) for 10 min, washed with PBS, and incubated with Fluoroshield™ Mounting Medium with DAPI (Sigma Aldrich, Missouri, USA). Images were processed using Adobe Photoshop CS6.

Data Pre-processing

Before augmentation the dataset included 216 images from six conditions: Normal Ca, 4 mM and 8 mM Ca, 16 mM Ca, 32 mM Ca, 16 mM Ca+ATP, and 32 mM Ca+ATP. Images were stored in JPEG format with a resolution of 2592 x 1944. Data augmentation was applied to the raw images using the following transformation techniques: 40 degrees image rotation, shear_range = 0.2, zoom_range = 0.2, horizontal flipping, and modifying image brightness. This produced a total of 4587 train images and 1379 test images considering all six conditions. Data augmentation is used to increase the diversity of a dataset by randomly creating new slightly modified versions of the instances that are already present in the dataset. After splitting the dataset into training and testing, the model was built according to the following architecture: four convolutional layers, three max-pooling layers, one flatten layer, three dense layers with the last one being a softmax layer containing six neurons applied to classify the cell images into the defined six categories. The network parameters were configured as follows: Adam optimizer [19], activation = "ReLu", input shape = 128, 128, 1, batch size: 64, epochs: 25, verbose=1, sparse_categorical_crossentropy loss, n_splits: 10, n_repeats: 3. Early stopping was applied with patience value =5 for maximum value for validation accuracy. The neural network training was performed with Keras using TensorFlow version 2.5.0 [20] on Intel(R) Core(TM) i7-10700T CPU @ 2.00GHz.

Real Time-PCR

Total RNA extraction from HK-2 cells was done using the RNeasy Mini kit (Qiagen, Valencia, CA, USA). cDNA was generated from total RNA using FIREScript RT cDNA Synthesis KIT (Solis BioDyne, Tartu, Estonia) using random primers following the manufacturer's protocol. cDNA samples from all conditions were diluted to 10 ng/µl. Real-time quantitative PCR was performed in StepOnePlus Real-Time PCR cycler (Applied Biosystems, Foster City, CA) using 5x HOT FIREPol® EvaGreen® qPCR Supermix kit (Solis BioDyne, Tartu, Estonia). The cycling conditions were as follows: Initial activation at 95°C for 12 minutes, followed by 40 cycles at 95°C for 15 seconds, annealing at 53^0C for 30 seconds, elongation at 72°C for 30 seconds. GAPDH was used as the reference gene, and fold change in gene expression was calculated using the comparative CT (2-ΔΔCT) method. The relative mRNA abundance was obtained by the ratio of fold change of sample to control. Primers for tested genes were as follows:

GAPDH: forward 5'-TCGGAGTCAACGGATTTGG-3' and reverse 5'-GCAACAATATCCACTTTACCAGAGT-TAA-3'; Calmodulin: forward 5'-GGCATTCCGAGTCTTTGACAA-3' and reverse 5'-CCGTCTCCATCAATATCT-GCT-3'; S100A8: forward 5'-GGGATGACCTGAAGAAATTGCTA-3' and reverse 5'-TGTTGATATCCAACTCTTT-GAACCA-3'; S100A14: 5'-GTCGGTCAGCCAACGCAGAG-3' and reverse 5'-CAGGCCACAGTTGCTCGG-3'; CaBP-28k: forward 5'-AGT GGT TAC CTG GAA GGA AAG G-3' and reverse 5'-AGT GGT TAC CTG GAA GGA AAG G-3'; P21: forward 5'-CATGTGGACCTGTCACTGTCTTGTA-3' and reverse 5'-GAAGATCAGCCGGCGTTTG-3'; Mcl-1: forward 5'-ATGCTTCGGAAACTGGACAT-3' and reverse 5'- TCCTGATGCCACCTTCTAGG-3'.

Statistical analysis

The results are reported as means ± SEM from at least three independent experiments. One-way analysis of variance followed by Tukey's test for pairwise comparisons were used to estimate statistically significant differences between the control and treatments and plotted using GraphPad Prism 5. For analysis between two groups, Student's t-test was used. p values represented as follows: *($p < 0.05$), **($p < 0.01$), and *** ($p < 0.001$).

Results

High levels of extracellular calcium decrease the viability of human proximal kidney (HK-2) cells

To investigate the effect of elevated extracellular calcium on the viability of human proximal kidney cells, we compared the viability of HK-2 cells cultured in normal media and media supplemented with increasing amounts of calcium chloride. Cells were cultured in the media containing normal levels of calcium (1.8 mM) and media with increasing concentrations of calcium (4 mM Ca, 8 mM Ca, 16 mM Ca, 32 mM Ca, and 64 mM Ca) for 18-20 hours and viability was determined by light microscopy (Optika) (Fig. 1A), and MTT assay (Fig. 1B). Morphologically, cells treated with 4 mM Ca and 8 mM Ca, were similar to cells cultured in normal Ca (Fig. 1A). Cells treated with 16 mM Ca showed increased signs of cell death, such as cell detachment, rounding, and shrinkage. These changes were intensified with increased calcium concentrations (32 mM Ca and 64 mM Ca) (Fig. 1A). Consistent with morphological changes, the MTT assay revealed a significant reduction in viability of cells starting at 16 mM Ca and increased in a dose-dependent manner, compared to cells in normal Ca, 4 mM Ca, and 8 mM Ca (Fig. 1B).

Extracellular ATP protects HK-2 cells against high elevated extracellular calcium levels

Previous studies in cancer cells reported that the extracellular ATP acts via purinergic receptors to regulate several cellular events such as cell proliferation, differentiation, and apoptosis [21, 22]. Thus, we have investigated the effect of extracellular ATP on the viability of HK-2 cells cultured in elevated calcium levels by using light microscopy, MTT assay, and nuclear morphology using DAPI staining (Fig. 2). Morphological analysis revealed that the treatment of cells with ATP (50 µM) enhanced the survival of HK-2 cells cultured in elevated calcium levels (16 mM and 32 mM Ca), compared with cells without ATP (Fig. 2A). To further confirm ATP-mediated protection of HK-2 against elevated calcium levels, nuclear changes

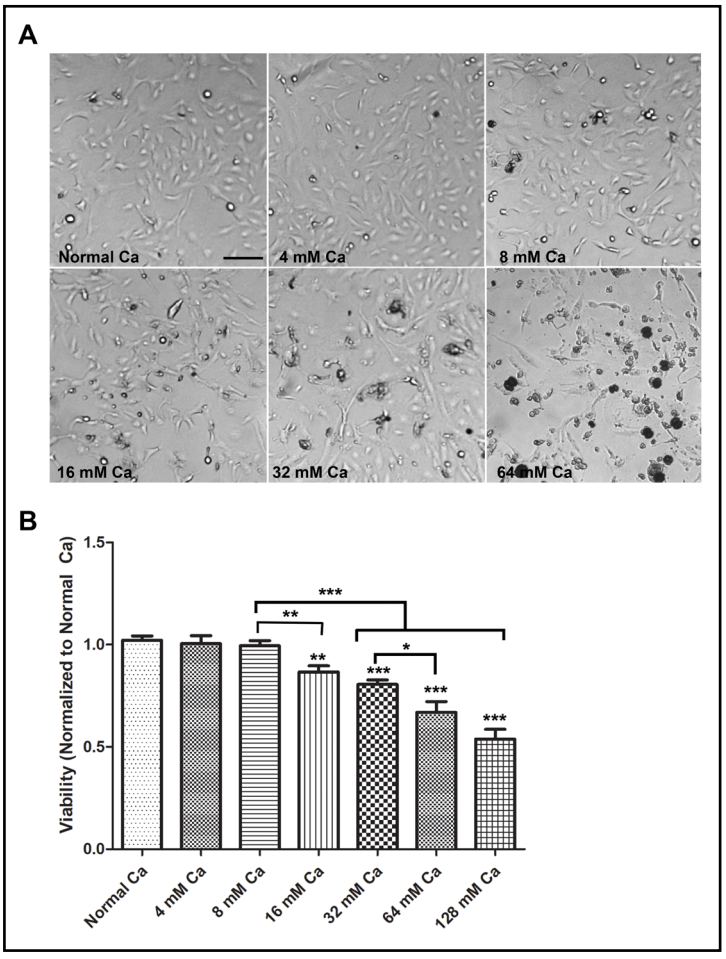

Fig. 1. Dose-dependent decrease in the viability in response to elevated extracellular calcium in human proximal kidney (HK-2) cells. A. Light microscopy of HK-2 cells cultured in normal Ca or elevated concentrations of extracellular [Ca^{2+}] (4 mM Ca, 8 mM Ca, 16 mM Ca, 32 mM Ca, 64 mM Ca) for 18-20 h. Cells were photographed with an inverted microscope (Optika) (scale, 100 µm). B. MTT analysis of HK-2 cells treated as in A. After treatment, cell viability was determined using MTT Assay. Data are represented as normalized MTT activity to cells cultured in normal Ca. Bar graphs represent mean ±SEM of three independent experiments. Statistically significant differences were determined by one-way ANOVA. Statistical comparison between two conditions was performed using t-test, *p <0.05, **p <0.01, ***p <0.001.

were examined by DAPI staining. As shown in Fig. 2B, nuclear fragmentation, nuclear condensation, and nuclear shrinkage were apparent in cells treated with 16 mM and 32 mM Ca. However, few changes were observed in the cells cultured in normal calcium, where cells displayed normal nuclear morphology. Cells treated with 16 mM or 32 mM Ca, in the presence of ATP, showed fewer signs of nuclear changes, suggesting ATP protection against damage by elevated extracellular calcium (Fig. 2B).

MTT analysis results demonstrated that ATP significantly protects HK-2 cells cultured in 16 mM and 32 mM Ca, compared to cells in similar conditions but with no ATP (Fig. 2C). Cells cultured in normal calcium and treated with ATP showed a significant increase in cell proliferation, compared to control cells (Fig. 2C).

ATP-mediated protection of HK-2 cells against high extracellular Ca^{2+} is associated with regulation of intracellular $[Ca^{2+}]_i$

To study the changes in intracellular calcium ion in cells cultured in elevated extracellular [Ca^{2+}], we monitored intracellular $[Ca^{2+}]_i$ changes using a fluorescent Ca^{2+} indicator (Fluo-4 AM) in cells cultured in high extracellular calcium (16 mM and 32 mM Ca), in the presence and absence of ATP (Fig. 3). Fluorescence microscopy was used to observe alterations in free intracellular Ca^{2+} levels. As shown in Fig. 3, cells cultured in 16 mM Ca and 32 mM Ca demonstrated an increase in $[Ca^{2+}]_i$, compared to $[Ca^{2+}]_i$ levels in cells cultured in normal calcium. The increased $[Ca^{2+}]_i$ observed in 16 mM and 32 mM Ca was attenuated in cells treated with ATP, suggesting regulation of intracellular calcium homeostasis (Fig. 3, lower row).

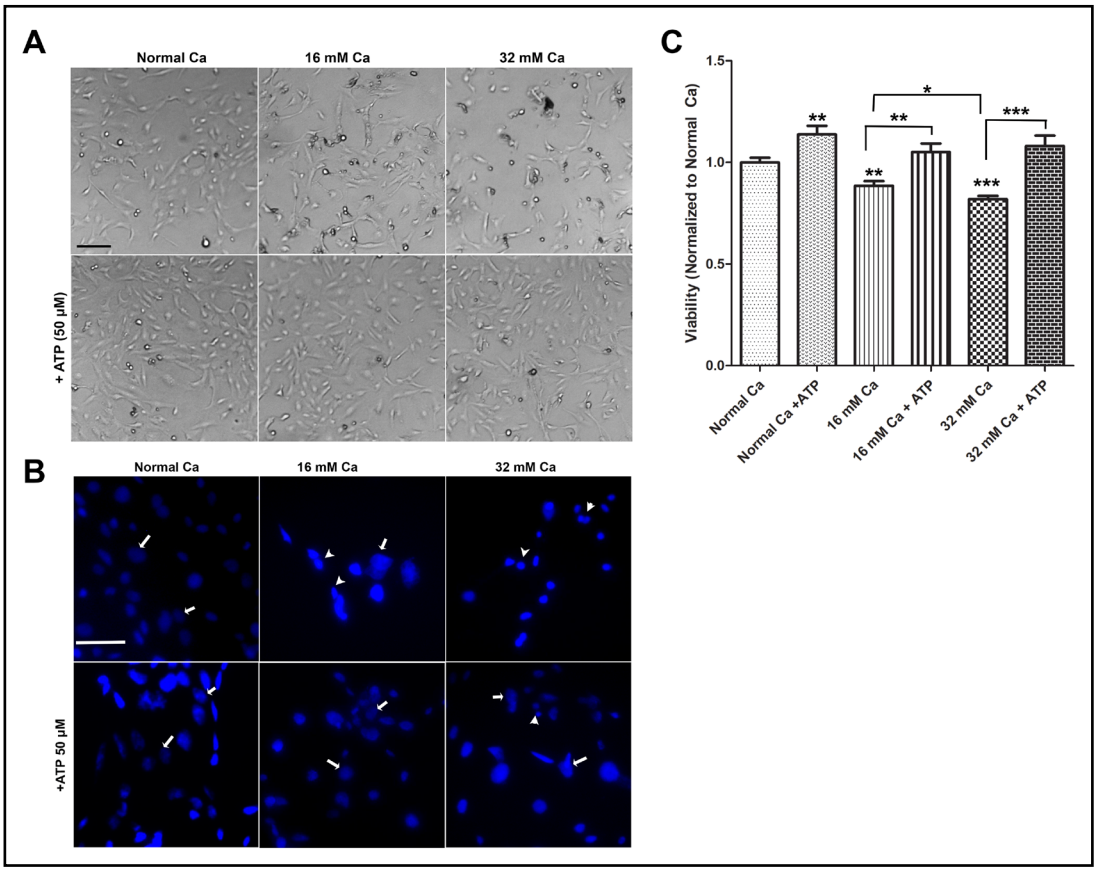

Fig. 2. Extracellular ATP protects HK-2 cells against elevated extracellular calcium. A: light microscopy of HK-2 cells before harvest. HK-2 cells were cultured in normal calcium (Normal Ca) or cultured in 16 mM Ca or 32 mM Ca for 18-20 h. Similar cells were treated with ATP (50 µM). Cells were photographed with an inverted microscope (Optika) before harvesting (scale, 100 µm). B. Representative fluorescent images of HK-2 cells after DAPI staining. Cells were cultured on glass-bottom plates before treated as in A. Cells were then fixed with 4 % paraformaldehyde, and stained with DAPI. Nuclear changes were studied with a fluorescence microscope with DAPI filter. White arrows indicate normal nuclei, and white arrowheads indicate damaged nuclei. C: CyQUANT™ MTT Cell Proliferation Assay analysis of HK-2 cells treated as in A. Results show cell viabilities normalized to normal Ca. Bar graphs represent mean ±SEM of three independent experiments. Statistically significant differences were determined by one-way ANOVA. Statistical comparison between two conditions was performed using t-test, *p <0.05, **p <0.01, ***p <0.001.

Fig. 3. Modulation of intracellular $[Ca^{2+}]_i$ levels by ATP in response to elevated extracellular Ca in HK-2 cells. C. Cells seeded on glass-bottom dishes were cultured in 16 mM Ca or 32 mM Ca, in the presence or absence of ATP for 18 h, and incubated with the fluorescent calcium dye, Fluo-4 AM. Calcium signal in the cytosol were observed by Optika XDS-2 inverted fluorescence microscope using FITC filter.

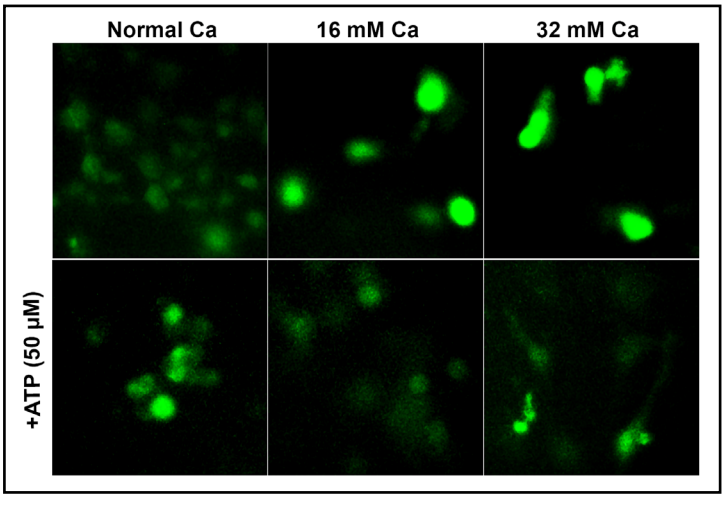

Convolutional Neural Network-Based Model Obtained on Light Microscopy Data

In order to automate and speed up the overall classification process of light microscopy images of HK-2 cells cultured in elevated extracellular calcium, we sought to use CNN based technique. Such models offer high efficiency in image classification and detection [23, 24]. Transmitted light microscopy images for HK-2 cells cultured in normal Ca, 4 mM Ca and 8 mM Ca, 16 mM Ca, 32 mM Ca, 16 mM Ca with ATP (16mM Ca+ATP), and 32 mM Ca with ATP (32 mM Ca+ATP), were used to train CNN model based on the architecture discussed in the material and methods (Fig. 4). Incremental learning of our CNN model through each epoch was assessed by Model accuracy (Fig. 5A), Loss function (Fig. 5B) in the training and testing data sets, and ROC curve for classification performance (Fig. 5C). Loss function is defined as

$$\mathrm{LCE} = -\sum_{i=1}^{n} t_i \log(p_i), for\ n\ classes,$$

where t_i is the truth label and p_i is the Softmax probability for the i^{th} class.

The accuracy of model performance on the training dataset and test dataset were 97% and 98%, respectively, and F-score of 0.98.

The final goal in this scenario was to train a model that is able to identify cell survival of HK-2 cells cultured in elevated [Ca^{2+}] conditions, in the presence or absence of ATP, based on a simple, fast and accurate classification of morphological changes in culture using light microscopy images. Pairwise comparisons resulted in a diagonally-populated confusion matrix indicating that our model was capable of identifying cell-specific features to correctly discriminate all labels (Fig. 5D and 5E).

The correct predictions of cells cultured in 16 mM Ca was 465 out of 467. The two remaining images were misclassified as 32 mM Ca, which also represent injured cells, suggesting high accuracy of the model to discriminate between injured cells and normal cells. Similarly, in cells cultured in 32 mM Ca, 206 out of 208 images were correctly predicted, with one image predicted as 16 mM Ca and one image predicted as 4 mM or 8 mM Ca. (Fig. 5D and 5E). The correct predicted cells cultured in 16 mM Ca with ATP (16 mM Ca+ATP) were 412 out of 414. The two misclassified images were predicted as cells cultured in normal Ca. Importantly, none of the images in the protected groups (16 mM Ca+ATP and 32 mM Ca+ATP) were misclassified as 16 mM or 32 mM Ca, suggesting the high performance of our model to discriminate injured cells from protected cells. Similarly, the correctly predicted

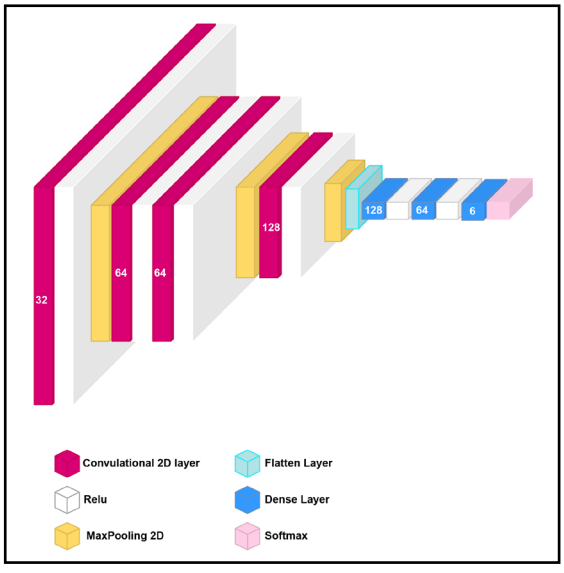

Fig. 4. Architecture of the convolutional neural network (CNN). The CNN consists of four convolutional layers, three max-pooling layers, one flatten layer, three dense layers with the last one being a softmax layer connected to six neurons applied to classify the cell images into the defined six categories. The input shape was set to (128,128,1) and the activation function used was ReLu. 10-fold cross validation was applied with 3 repeats.

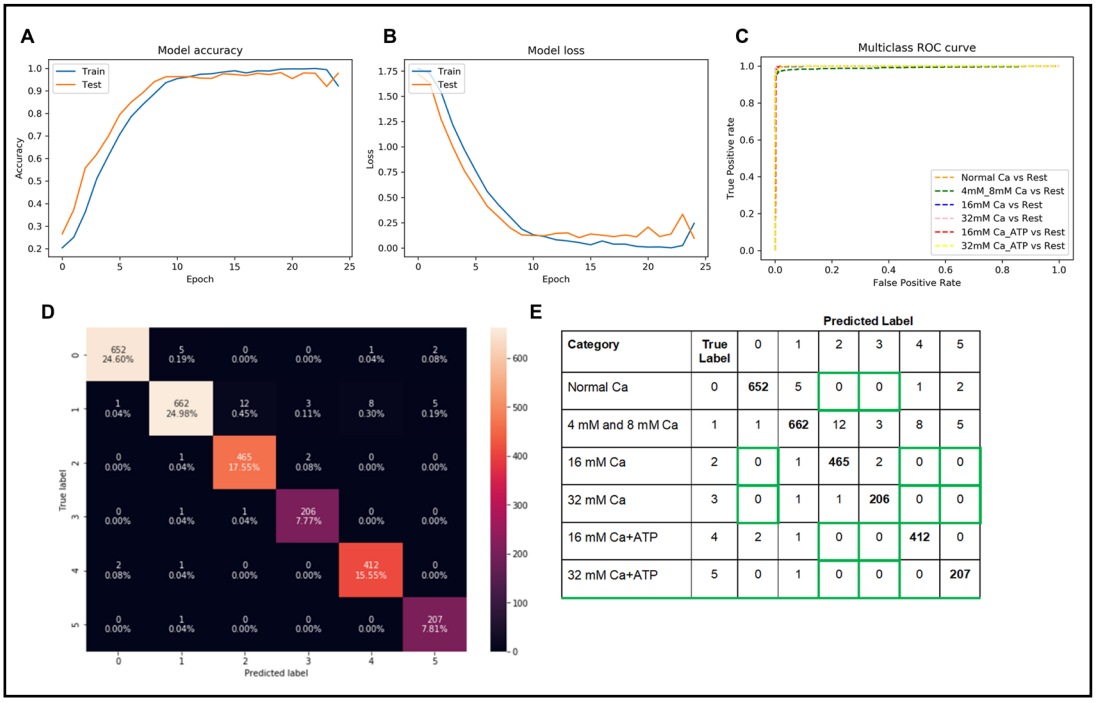

Category	True Label	0	1	2	3	4	5
Normal Ca	0	**652**	5	0	0	1	2
4 mM and 8 mM Ca	1	1	**662**	12	3	8	5
16 mM Ca	2	0	1	**465**	2	0	0
32 mM Ca	3	0	1	1	**206**	0	0
16 mM Ca+ATP	4	2	1	0	0	**412**	0
32 mM Ca+ATP	5	0	1	0	0	0	**207**

Fig. 5. Machine learning algorithm for prediction of survival of HK-2 cells cultured in high extracellular calcium. A. Training and testing accuracy (A) and training and testing loss (B) plots, and ROC curve (C) achieved by the CNN model. D. Confusion matrix and heatmap of CNN model tested in the test dataset. E. Confusion matrix with labels of CNN model when tested on the test dataset. The CNN model also performed very efficiently giving correct classification results as can be seen in the results where none of the images in 16 mM Ca or 32 mM Ca (injured cells) were falsely classified as normal or protected by extracellular ATP (cells with green boundaries).

images of cells cultured in 32 mM Ca with ATP (32 mM Ca+ATP) were 207 out of 208, with one misclassified image as normal Ca, and no predicted images as 16 mM Ca or 32 mM Ca.

Finally, we tested the accuracy of our model with eight images that were not included in training or test data of the model. Four images were from cells cultured in 16 mM Ca with ATP and four images from cells in 32 mM Ca with ATP (Fig. 6). The model correctly predicted all four images from cells in 16 mM Ca with ATP (Fig. 6A). Cells in 32 mM Ca with ATP were predicted as protected (32 mM Ca with ATP or 16 mM Ca with ATP) and one image were misclassified as 4 and 8 mM Ca (Fig. 6B), which are also known to be uninjured cells based on our previous viability results (Fig. 1).

ATP-mediated protection of HK-2 against elevated extracellular [Ca^{2+}] is associated with an increase in calmodulin, S100A8, S100A14, and calbindin-D28k (CaBP28k) expression

Calcium-binding proteins play a vital role in the regulation of calcium homeostasis and signalling through diverse mechanisms, including modulation of intracellular calcium levels and transduction of intracellular [Ca^{2+}] signals [25, 26]. CaBPs can also regulate energy metabolism, enzyme activity, cell proliferation and differentiation [27-29]. In particular, the deregulated expression of calmodulin, S100A8, S100A14, calbindin-D28k (CaBP28k) has been associated with cell survival and apoptotic pathways in several cancer models [30-33]. In this study, we assessed the expression of these genes in HK-2 cells cultured in elevated extracellular calcium levels. Cells cultured in the media with 16 mM Ca showed a significant increase in S100A8, S100A14, and CaBP28k mRNA levels, compared to cells cultured in normal Ca. The increase in the expression of S100A14 and CaBP-28k genes was dose-dependent as shown by a 4-fold and 5-fold increase in mRNA levels in cells cultured in 32 mM Ca, as compared to 1.5-fold and 2-fold increase at 16 mM, respectively (Fig. 4).

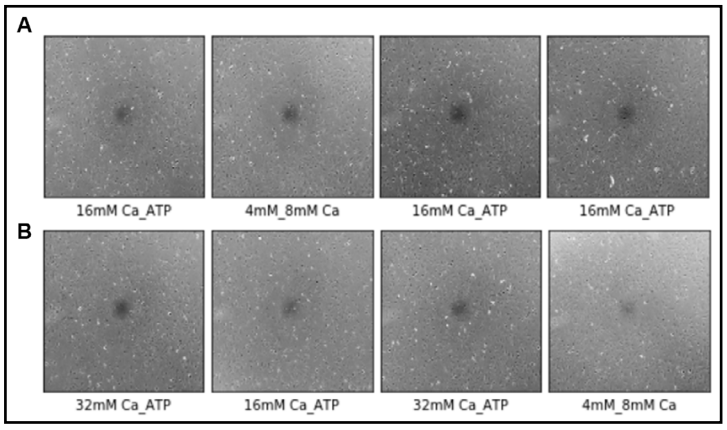

Fig. 6. Model performance on unseen images. Eight images from protected cells (16mM Ca+ATP and 32 mM Ca+ATP) that were not included in training or test data of the model. (A). Four images were from cells cultured in 16 mM Ca with ATP (upper row). (B). four images from cells in 32 mM Ca with ATP (lower row). The model correctly predicted three out of four images from cells in 16 mM Ca+ ATP (upper row). Two images in 32 mM Ca+ATP were predicted 32 mM Ca+ATP (protected), one image as 16 mM Ca+ATP (protected), one image as 4_8 mM Ca (uninjured). None of the images were classified as injured calls (16 mM Ca or 32 mM Ca).

Interestingly, the mRNA levels of S100A8 at 32 mM and 16 mM Ca were similar, suggesting a differential modulation of this CaBP. Calmodulin mRNA levels at 16 mM Ca were similar to the control. However, at 32 mM Ca showed a significant increase (2.9-fold), compared to cells in normal Ca.

We next sought to study the changes, in the presence of ATP, for the expression of calmodulin, S100A14, S100A8, and CaBP28k. Cells treated with ATP showed a significant increase in calmodulin (approximately 2.5-fold) expression compared to 16 mM Ca. Similarly, cells co-treated with 32 mM Ca and ATP showed a significant increase (approximately 2.5-fold) in calmodulin compared to 32 mM Ca alone. In the presence of ATP, the expression of S100A8 was increased (4.5-fold and 6-fold) in HK-2 cells cultured in 16 mM Ca and 32 mM Ca, compared to the conditions without ATP (Fig. 4). S100A14 mRNA levels were increased (3.4-fold and 2.9-fold) in cells cultured in 16 mM Ca and 32 mM Ca, in the presence of ATP. Similarly, CaBP28k mRNA levels were increased (3.5-fold and 5.4-fold), respectively, in cells cultured in 16 mM Ca and 32 mM Ca, in the presence of ATP, compared to similar conditions in the absence of ATP. Interestingly, the expression of calmodulin, S100A8, S100A14, and CaBP28k showed a significant increase in cells grown in normal calcium and treated with ATP (Fig. 7).

ATP-mediated protection of HK-2 cells against elevated extracellular [Ca^{2+}] is associated with an increase in cyclin-dependent kinase inhibitor p21, and anti-apoptotic protein, Mcl-1 expression

P21, a cyclin-dependent kinase inhibitor, was demonstrated to be induced in several models of acute kidney injury [34, 35]. This induction mediates cell cycle arrest after damage. In addition, it modulates apoptosis and necrosis [34]. Cells cultured in 16 mM Ca and 32 mM Ca demonstrated as significant increase (2.3-fold and 9.5 fold), respectively, in p21 expression. Cells cultured in 16 mM Ca and treated with ATP demonstrated a further increase in p21 levels (3.2-fold), compared to 16 mM Ca. Similarly, p21 mRNA levels in 32 mM Ca were induced with ATP (approximately 2-fold), compared to 32 mM Ca.

Next, we have investigated the expression of Mcl-1, an antiapoptotic protein [36]. Data showed approximately a 2-fold increase in Mcl-1 levels at 16 mM and 32 mM Ca. In the presence of ATP, Mcl-1 levels were doubled (2-fold) at 16 mM Ca, compared to 16 mM Ca. Similarly, mRNA level of Mcl-1 was induced (4-fold) in cells in 32 mM Ca, in the presence of ATP (Fig. 8).

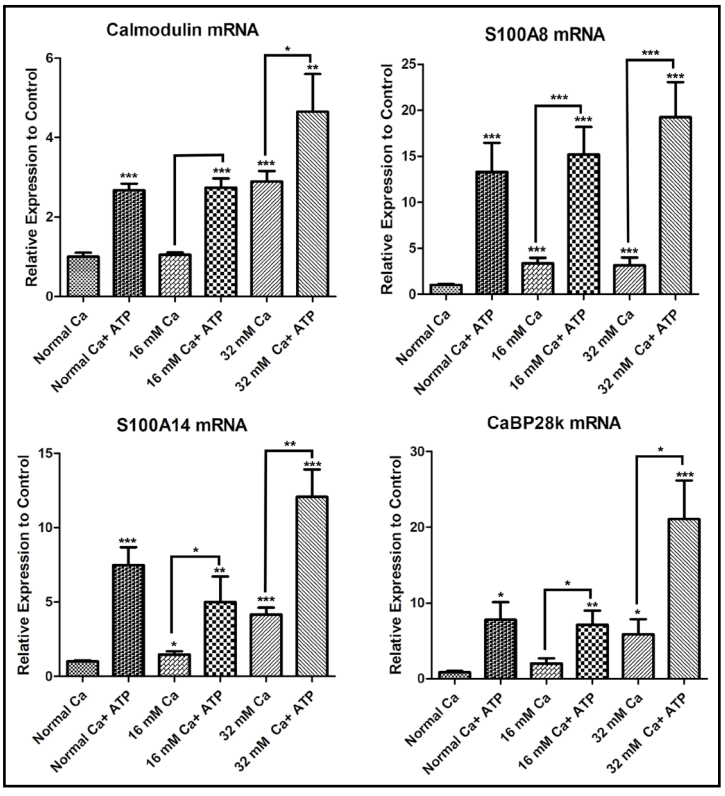

Fig. 7. Extracellular ATP enhanced expression of mRNA of calcium-binding proteins, calmodulin, S100A8, S100A14, and calbindin-D28k (CaBP28k). After treatment, total RNA was extracted from cells followed by cDNA synthesis and real-time qPCR. All mRNA expression levels were normalized against GAPDH. Each value is the mean ± SEM from three independent experiments. Statistically significant differences were determined by one-way ANOVA. Statistical significance between two conditions was performed using t-test, *p <0.05, **p <0.01, ***p <0.001.

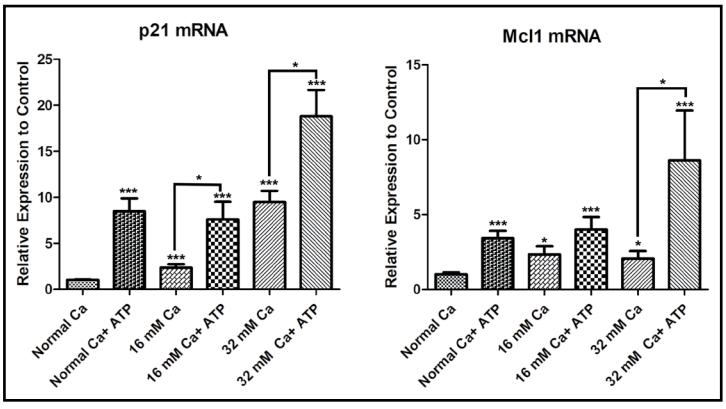

Fig. 8. Extracellular ATP enhanced expression of p21 and Mcl-1. Total RNA was isolated from treated cells followed by cDNA synthesis and real-time qPCR. All mRNA expression levels were normalized against GAPDH. Each value is the mean ± SEM from three independent experiments. Statistically significant differences were determined by one-way ANOVA. Statistical comparison between two conditions was performed using t-test, *p <0.05, ***p <0.001.

Discussion

Several studies showed that kidney stones formation is positively correlated to supersaturation for calcium oxalate or phosphate in urine and that hypercalciuria is present in 25–60% of stone formers [37, 38]. Other *in vivo* and *in vitro* studies reported excessive generation of ROS and subsequently oxidative stress-induced injury in HK-2 cells cultured in high extracellular calcium [39, 40]. Zhao et al. used an *in vitro* model of HK-2 cells exposed to increasing concentrations of CaCl2 to resemble the hypercalciuria environment *in vivo*. This study demonstrated cell injury of these cells through apoptosis, autophagy, and inflammatory processes [41]. Several other studies reported overproduction of ROS in renal tubular epithelial cells exposed to calcium crystals followed by cellular injury [42-45]. The oxidative stress is also linked with mitochondrial damage and alterations of intracellular

calcium homeostasis [46, 47]. However, the association between high extracellular calcium, cytosolic calcium, and transduction of [Ca^{2+}] signaling in these cells were not studied.

Although several studies have reported intracellular ATP depletion in renal proximal cells triggered by severe oxidative stress, extracellular ATP was shown to enhance survival against oxidative stress in other cell types [48]. Extracellular ATP can stimulate proliferation and differentiation in a variety of cells [49].

Our study investigated the effect of extracellular ATP on survival of HK-2 cells cultured in elevated extracellular calcium levels. Initially, we assessed morphological changes and viability in HK-2 cells cultured in increasing amounts of calcium chloride. Starting from 16 mM Ca we detected morphological signs of cell death in these cells after 18-20 hours incubation (Fig. 1A). The signs of injury increased with increased dose of CaCl2. The morphological changes were confirmed by proliferation assay showing significant dose-dependent decrease in viability of HK-2 starting at 16 mM Ca (Fig. 1B). No obvious morphological changes or significant reduction in cell viability was detected in cells cultured at 4 mM and 8 mM Ca, compared to normal Ca. For studying the effect of extracellular ATP, we selected conditions at 16 mM and 32 mM Ca based on significant decrease in HK-2 cells viability at these concentrations. We showed that the supplementation of media with ATP (50 μM) completely protects cells from injury against high extracellular calcium (Fig. 2). Our results support previous studies demonstrating ATP-mediated stimulation of proliferation in other types of epithelial cells [50, 51]. Extracellular ATP can bind various P2-purinergic cell surface receptors to modulate various cell functions, including cell proliferation and apoptosis [52]. Some studies reported extracellular ATP modulation of essential yet opposing cellular processes in the same cell type. In glomerular mesangial cells, extracellular ATP stimulated cell proliferation through P2Y receptors while conversely promoted apoptosis and necrosis via P2X receptors [51, 52].

Based on previous studies associating extracellular ATP with changes in intracellular [Ca^{2+}]$_i$ [53], we monitored [Ca^{2+}]$_i$ in conditions with elevated extracellular Ca, in the presence and absence of ATP, with Fluo-4 AM. Our results demonstrated an increase in Fluo-4 AM intensity in cells cultured at 16 mM and 32 mM Ca, consistent with previous studies showing activation of calcium-sensing receptor by an increase in extracellular Ca^{2+} and subsequent increase in [Ca^{2+}]$_i$ in renal epithelial cells [10, 53]. Cells cultured in 16 mM Ca and 32 mM Ca and exhibiting protection by ATP showed a decrease in Fluo-4 AM intensity as compared to cells without ATP (Fig. 3). Cells cultured in normal calcium with ATP show slight increase of Fluo-4 AM signals, consistent with reports linking ATP to mobilization of Ca from ER stores. The increase in Fluo-4 AM in cells treated with 16 mM and 32 mM Ca was attenuated with extracellular ATP. This suggest that extracellular ATP modulates intracellular [Ca^{2+}]$_i$ in 16 mM and 32 mM Ca, which could be a potential cause for promoting cell survival under these conditions.

CaBPs are important modulators of intracellular calcium dynamics of CaBP and thus they contribute to numerous cellular functions, including proliferation, differentiation, apoptosis, energy metabolism, and enzyme activity [54-56]. We sought to study the expression of selected CaBP, calmodulin, S100A8, S100A14, and CaBP-28k. These CaBPs were reported in different models of injury of normal renal epithelial cells [57-61]. We found that cells cultured at 16 mM Ca showed significant increase in mRNA levels of S100A8, S100A14, and CaBP28k, compared to cells cultured in normal calcium (Fig. 7). Further increases in mRNA levels were detected for these proteins at 32 mM Ca. While calmodulin mRNA levels were also increased at 32 mM, no change in mRNA levels at 16 mM Ca, suggesting differential regulation of these proteins by elevated extracellular calcium. Moreover, we showed that the mRNA levels of calmodulin, S100A8, S100A14, and CaBP28k were further upregulated by ATP in cells cultured in elevated calcium (16 mM and 32 mM Ca). Similarly, cells cultured in normal Ca showed enhanced expression for calmodulin, S100A8, S100A14, and CaBP28k. Our results suggest a positive correlation between expression of CaBPs and protection of HK-2 cells against elevated extracellular calcium, consistent with the known role of these calcium binding proteins as important modulators of intracellular calcium.

Although the exact mechanism by which CaBPs are involved in ATP-mediated protection requires further investigation, it is possible that upregulated CaBPs act as Ca^{2+} buffers to abnormal increase in $[Ca^{2+}]_i$, which maintain Ca^{2+} homeostasis and cell survival [62]. It is also possible that CaBPs are involved through their role as Ca transducers in important processes including cell proliferation and apoptosis [26].

Further, P21 mRNA levels in cells cultured at 16 mM and 32 mM Ca with ATP was induced to higher levels compared to conditions without ATP. This suggests a positive role for p21 in ATP-mediated protection. Our finding supports previous studies showing p21 enhanced cell survival in several models of AKI [63-66]. We also found significant induction of anti-apoptotic protein, Mcl-1, in cells treated with ATP, suggesting a positive role for Mcl-1 in ATP-mediated protection against elevated extracellular calcium.

Our studies present an *in vitro* model to study cell injury by elevated extracellular calcium in the proximal tubule region, a primary site for injury in acute and chronic kidney diseases. This is attributed to the fact that the proximal cortical tubule make up most of the kidney cortical mass and to their increased sensitivity to several insults, including kidney stones [67]. Although several other studies reported injury of renal epithelial cells by elevated extracellular calcium, we showed for the first time that extracellular ATP protects against elevated extracellular calcium in human proximal kidney cells. Furthermore, we showed differential modulation of expression of CaBPs, cell cycle inhibitor, and antiapoptotic Mcl-1, in cells cultured in the presence of extracellular ATP. We suggest that our study is helpful in dissection of mechanisms involved in protection of proximal cells against injury by elevated calcium levels. Studying cell viability in HK-2 cells is central aspect in any additional studies needed to explore the levels of extracellular calcium in renal cells. The fact that biochemical methods used to detect injury and survival of cells in culture continue to have several difficulties such as time commitment, considerable cost, sensitivity depending on identifying the type of cell death, acquired technical expertise, and low throughput of several assays, we decided to implement artificial intelligence and deep learning using light microscopy images to detect cell fate of HK-2 cells in elevated extracellular Ca conditions. We have proposed a CNN-based analysis and classification method (Fig. 6) which provided high accuracy on train (97%) and test data (98%). In addition to this model, we performed two other models: model b with increased batch size, and model c with increased k-folds (Table 1). Despite slight differences in runtime, the best classification was obtained with model a, compared to model b and c. The confusion matrix of the network performance using model a showed only one image of cells in 16 mM Ca misclassified as 4 and 8 mM Ca, and two images of cells in 16 mM Ca misclassified as 32 mM Ca. Importantly, none of the images at 16 mM Ca were misclassified as normal or protected HK-2 (16 mM Ca+ATP and 32 mM Ca+ATP). Similarly, only two images in 32 mM Ca were misclassified in 4 mM Ca and 8 mM Ca and 16 mM Ca, respectively. The model demonstrated high performance in classification of injured cells compared to normal and cells protected by extracellular ATP. None of the cells in the categories with extracellular ATP were classified as injured cells (16 mM and 32 mM Ca). To further test our model a on unseen data, we classified four random images from 16 mM Ca+ATP and four images from 32 mM Ca+ATP using model a. Three out of four images from cells cultured at 16 mM Ca+ATP, and previously unseen, were classified in 16 mM Ca+ATP group. Images from 32 mM Ca+ATP were classified as protected

Table 1. Comparison of three models (a, b, and c) based on accuracy and loss function of training and testing dataset

Model	Kfolds	Repeats	BatchSize	Epochs	Time	Train Dataset		Test Dataset	
						Accuracy	Loss	Accuracy	Loss
a	10	3	64	25	17h54m	97	0.13	98	0.13
b	10	3	128	25	18h50m	97	0.14	98	0.12
c	5	5	64	25	13h51m	93	0.33	95	0.22

groups with one image misclassified as 4mM Ca and 8 mM Ca. Our results demonstrated high performance for our CNN-model for prediction of injury and protection of HK-2 cells against elevated extracellular calcium.

Conclusion

Our study demonstrated dose-dependent injury of HK-2 cells against elevated extracellular calcium, which can be protected by extracellular ATP. Elevated levels of extracellular calcium are associated with increase in intracellular calcium, which is suppressed in the presence of ATP. We also demonstrated an induction of CaBPs, calmodulin, S100A8, S100A14, and CaBP28k in injured cells by elevated Ca and much dramatic increase in the presence of ATP, suggesting a role for these proteins in modulation of cytosolic calcium during elevated extracellular calcium. In addition, our data also suggest that this effect of ATP-mediated protection may be exerted via induction of p21, and Mcl-1. Finally, we introduced a deep learning based CNN model to successfully classify HK-2 cells images that are injured and ATP-protected using an easy, rapid, and inexpensive means of measuring cellular injury of human proximal kidney cells. However, this method has few limitations. First, significant amount of time spent on the image acquisition. Next, since the histological tissue slides derived from patients usually contains different types of cell, our study results cannot be directly implemented into clinical environment. However, recent advances in imaging methods can improve the speed of image acquisition and the quality of input images. This will create opportunities for deploying CNN based techniques in the field of biomedicine. This study has demonstrated the feasibility of performing classification task of kidney cells with 98% accuracy.

Acknowledgements

This research was supported by the Department of Biotechnology at the American University of Ras Al Khaimah. We are grateful to the Office of Research and Community Service at AURAK for the excellent help with purchasing orders. We thank AURAK Biotechnology students Ridhi Bhudia and Nejood Alshehhi for their assistance with cell culture.

Author Contributions

R.H. (conceptualization, performing experiments, data collection, formal analysis, funding acquisition, and writing). A.G. (conceptualization, methodology, formal analysis, supervision, validation, and writing). C.G.V., R.M., and M.M. (resources, review & editing). J.M. and H.A.Z. (resources, review & editing). All authors read and approved the final manuscript.

Funding

This work was supported by a grant from the American University of Ras Al Khaimah (AURAK) (SEEDGRANT: Ref No: AAS/002/20 to R.H.).

Disclosure Statement

The authors have no conflicts of interest to declare.

References

1 Gorkhali R, Tian L, Dong B, Bagchi P, Deng X, Pawar S, Duong D, Fang N, Seyfried N, Yang J: Extracellular calcium alters calcium-sensing receptor network integrating intracellular calcium-signaling and related key pathway. Sci Rep 2021;11:1-16.
2 Berridge MJ: Calcium signalling in health and disease. Biochem Biophys Res Commun 2017;485:5.
3 Tiselius HG: A hypothesis of calcium stone formation: an interpretation of stone research during the past decades. Urol Res 2011;39:231-243.
4 Craven BL, Passman C, Assimos DG: Hypercalcemic States associated with nephrolithiasis. Rev Urol 2008;10:218-226.
5 Jones DB, Jones JH, Lloyd HJ, Lucas PA, Wilkins WE, Walker DA: Changes in blood pressure and renal function after parathyroidectomy in primary hyperparathyroidism. Postgrad Med J 1983;59:350-353.
6 Kristoffersson A, Backman C, Granqvist K, Järhult J. Pre- and postoperative evaluation of renal function with five different tests in patients with primary hyperparathyroidism. J Intern Med 1990;227:317-324.
7 Thongprayoon C, Cheungpasitporn W, Chewcharat A, Mao MA, Bathini T, Vallabhajosyula S, Thirunavukkarasu S, Kashani KB: Impact of admission serum ionized calcium levels on risk of acute kidney injury in hospitalized patients. Sci Rep 2020;10:1-6.
8 Friedman PA, Gesek FA: Cellular calcium transport in renal epithelia: measurement, mechanisms, and regulation. Physiol Rev 1995;75:429-471.
9 Ng RH, Menon M, Ladenson JH: Collection and handling of 24-hour urine specimens for measurement of analytes related to renal calculi. Clin Chem 1984;30:467-471.
10 Vezzoli G, Macrina L, Magni G, Arcidiacono T: Calcium-sensing receptor: evidence and hypothesis for its role in nephrolithiasis. Urolithiasis 2019;47:23-33.
11 Verkoelen CF, van der Boom BG, Kok DJ, Houtsmuller AB, Visser P, Schröder FH, Romijn JC: Cell type-specific acquired protection from crystal adherence by renal tubule cells in culture. Kidney Int 1999;55:1426-1433.
12 Aihara K, Byer KJ, Khan SR: Calcium phosphate-induced renal epithelial injury and stone formation: involvement of reactive oxygen species. Kidney Int 2003;64:1283-1291.
13 Gombedza FC, Shin S, Kanaras YL, Bandyopadhyay BC: Abrogation of store-operated Ca2+ entry protects against crystal-induced ER stress in human proximal tubular cells. Cell Death Discov 2019;5:1-13.
14 Cao LC, Honeyman TW, Cooney R, Kennington L, Scheid CR, Jonassen JA: Mitochondrial dysfunction is a primary event in renal cell oxalate toxicity. Kidney Int 2004;66:1890-1900.
15 Williams J, Holmes RP, Assimos DG, Mitchell T: Monocyte Mitochondrial Function in Calcium Oxalate Stone Formers. Urology 2016;93:224.e1-e6.
16 Dominguez-Gutierrez PR, Kwenda EP, Khan SR, Canales BK: Immunotherapy for stone disease. Curr Opin Urol 2020;30:183-189.
17 Rizzuto R, De Stefani D, Raffaello A, Mammucari C: Mitochondria as sensors and regulators of calcium signalling. Nat Rev Mol Cell Biol 2012;13:566-578.
18 Bagur R, Hajnóczky G: Intracellular Ca2+ Sensing: Its Role in Calcium Homeostasis and Signaling. Mol Cell 2017;66:780-788.
19 Kingma DP, Ba J: Adam: A Method for Stochastic Optimization. ICLR 2015. URL: https://arxiv.org/abs/1412.6980.
20 Abadi M, Barham P, Chen J, Chen Z, Davis A, Dean J, Devin M, Ghemawat S, Irving G, Isard M, Kudlur M, Levenberg J, Monga R, Moore S, Murray DG, Steiner B, Tucker P, Vasudevan V, Warden P, Wicke M, et al.: TensorFlow: A System for Large-Scale Machine Learning, Proceedings of the 12th USENIX Symposium on Operating Systems Design and Implementation (OSDI '16) 2016. URL: https://www.usenix.org/system/files/conference/osdi16/osdi16-abadi.pdf.
21 Burnstock G, Knight GE: Cellular distribution and functions of P2 receptor subtypes in different systems. Int Rev Cytol 2004;240:31-304.
22 Song S, Jacobson KN, McDermott KM, Reddy SP, Cress AE, Tang H, Dudek SM, Black SM, Garcia JG, Makino A, Yuan JX: ATP promotes cell survival via regulation of cytosolic [Ca2+] and Bcl-2/Bax ratio in lung cancer cells. Am J Physiol Cell Physiol 2016;310:C99-C114.
23 Oei RW, Hou G, Liu F, Zhong J, Zhang J, An Z, Xu L, Yang Y: Convolutional neural network for cell classification using microscope images of intracellular actin networks. PLoS One 2019;14:e0213626.

24 Ghani A, Aina A, See CH, Yu H, Keates S: Accelerated Diagnosis of Novel Coronavirus (COVID-19)—Computer Vision with Convolutional Neural Networks (CNNs). Electronics 2022;11:1148.
25 Hermann A, Donato R, Weiger TM, Chazin WJ: S100 calcium binding proteins and ion channels. Front Pharmacol 2012;3:67.
26 Donato R: S100: a multigenic family of calcium-modulated proteins of the EF-hand type with intracellular and extracellular functional roles. Int J Biochem Cell Biol 2001;33:637-668.
27 Heizmann CW: The multifunctional S100 protein family. Methods Mol Biol 2002;172:69-80.
28 Huang Z, Fan G, Wang D: Downregulation of calbindin 1, a calcium-binding protein, reduces the proliferation of osteosarcoma cells. Oncol Lett 2017;13:3727-3733.
29 Jin QE, Chen H, Luo A, Ding F, Liu Z: Correction: S100A14 Stimulates Cell Proliferation and Induces Cell Apoptosis at Different Concentrations via Receptor for Advanced Glycation End Products (RAGE). Plos one 2016;11:e0147881.
30 Hodeify R, Siddiqui SS, Matar R, Vazhappilly CG, Merheb M, Al Zouabi H, Marton J: Modulation of calcium-binding proteins expression and cisplatin chemosensitivity by calcium chelation in human breast cancer MCF-7 cells. Heliyon 2021;7:e06041.
31 Jiang H, Hu H, Tong X, Jiang Q, Zhu H, Zhang S: Calcium-binding protein S100P and cancer: mechanisms and clinical relevance. J Cancer Res Clin Oncol 2012;138:1-9.
32 Emberley ED, Murphy LC, Watson PH: S100A7 and the progression of breast cancer. Breast Cancer Res 2004;6:153-9.
33 Coticchia CM, Revankar CM, Deb TB, Dickson RB, Johnson MD: Calmodulin modulates Akt activity in human breast cancer cell lines. Breast Cancer Res Treat 2009;115:545-560.
34 Price PM, Safirstein RL, Megyesi J: The cell cycle and acute kidney injury. Kidney Int 2009;76:604-613.
35 Megyesi J, Tarcsafalvi A, Li S, Hodeify R, Seng NS, Portilla D, Price PM: Increased expression of p21WAF1/CIP1 in kidney proximal tubules mediates fibrosis. Am J Physiol Renal Physiol 2015;308:F122-F130.
36 Yang-Yen HF: Mcl-1: a highly regulated cell death and survival controller. J Biomed Sci 2006;13:201-204.
37 Ratkalkar VN, Kleinman JG: Mechanisms of Stone Formation. Clin Rev Bone Miner Metab 2011;9:187-197.
38 Prochaska M, Taylor E, Ferraro PM, Curhan G: Relative Supersaturation of 24-Hour Urine and Likelihood of Kidney Stones. J Urol 2018;199:1262-1266.
39 Wang Y, Sun C, Li C, Deng Y, Zeng G, Tao Z, Wang X, Guan X, Zhao Y: Urinary MCP-1 HMGB1 increased in calcium nephrolithiasis patients and the influence of hypercalciuria on the production of the two cytokines. Urolithiasis 2017;45:159-175.
40 Khaskhali MH, Byer KJ, Khan SR: The effect of calcium on calcium oxalate monohydrate crystal-induced renal epithelial injury. Urol Res 2009;37:1-6.
41 Zhao J, Cheng J, Li C, Xu M, Ma C, Qin L, Yi K, Liao N: Ethyl Pyruvate Attenuates CaCl2-Induced Tubular Epithelial Cell Injury by Inhibiting Autophagy and Inflammatory Responses. Kidney Blood Press Res 2018;43:1585-1595.
42 Muthukumar A, Selvam R: Role of glutathione on renal mitochondrial status in hyperoxaluria. Mol Cell Biochem 1998;185:77-84.
43 Itoh Y, Yasui T, Okada A, Tozawa K, Hayashi Y, Kohri K: Preventive effects of green tea on renal stone formation and the role of oxidative stress in nephrolithiasis. J Urol 2005;173:271-275.
44 Zhai W, Zheng J, Yao X, Peng B, Liu M, Huang J, Wang G, Xu Y: Catechin prevents the calcium oxalate monohydrate induced renal calcium crystallization in NRK-52E cells and the ethylene glycol induced renal stone formation in rat. BMC Complement Altern Med 2013;13:228.
45 Li X, Ma J, Shi W, Su Y, Fu X, Yang Y, Lu J, Yue Z: Calcium Oxalate Induces Renal Injury through Calcium-Sensing Receptor. Oxid Med Cell Longev 2016;5203801.
46 Veena CK, Josephine A, Preetha SP, Rajesh NG, Varalakshmi P: Mitochondrial dysfunction in an animal model of hyperoxaluria: a prophylactic approach with fucoidan. Eur J Pharmacol 2008;579:330-336.
47 Niimi K, Yasui T, Okada A, Hirose Y, Kubota Y, Umemoto Y, Kawai N, Tozawa K, Kohri K: Novel effect of the inhibitor of mitochondrial cyclophilin D activation, N-methyl-4-isoleucine cyclosporin, on renal calcium crystallization. Int J Urol 2014;21:707-713.
48 Ahmad S, Ahmad A, Ghosh M, Leslie CC, White CW: Extracellular ATP-mediated signaling for survival in hyperoxia-induced oxidative stress. J Biol Chem 2004;279:16317-16325.
49 Lee YJ, Han HJ: Role of ATP in DNA synthesis of renal proximal tubule cells: involvement of calcium, MAPKs, and CDKs. Am J Physiol Renal Physiol 2006;291:F98-F106.

50 Schulze-Lohoff E, Zanner S, Ogilvie A, Sterzel RB: Extracellular ATP stimulates proliferation of cultured mesangial cells via P2-purinergic receptors. Am J Physiol 1992;263:F374-F383.
51 Harada H, Chan CM, Loesch A, Unwin R, Burnstock G: Induction of proliferation and apoptotic cell death via P2Y and P2X receptors, respectively, in rat glomerular mesangial cells. Kidney Int 2000;57:949-958.
52 Praetorius HA, Leipziger J: ATP release from non-excitable cells. Purinergic Signal 2009;5:433-446.
53 Toka HR: New functional aspects of the extracellular calcium-sensing receptor. Curr Opin Nephrol Hypertens 2014;23:352-360.
54 Elíes J, Yáñez M, Pereira TMC, Gil-Longo J, MacDougall DA, Campos-Toimil M: An Update to Calcium Binding Proteins. Adv Exp Med Biol 2020;1131:183-213.
55 Yáñez M, Gil-Longo J, Campos-Toimil M: Calcium binding proteins. Adv Exp Med Biol 2012;740:461-482.
56 Islam MS: Calcium Signaling: From Basic to Bedside. Adv Exp Med Biol 2020;1131:1-6.
57 López-Girona A, Bachs O, Agell N: Calmodulin is involved in the induction of DNA polymerases alpha and delta activities in normal rat kidney cells activated to proliferate. Biochem Biophys Res Commun 1995;217:566-574.
58 Tammaro A, Florquin S, Brok M, Claessen N, Butter LM, Teske GJD, de Boer OJ, Vogl T, Leemans JC, Dessing MC: S100A8/A9 promotes parenchymal damage and renal fibrosis in obstructive nephropathy. Clin Exp Immunol 2018;193:361-375.
59 Islam MN, Griffin TP, Sander E, Rocks S, Qazi J, Cabral J, McCaul J, McMorrow T, Griffin MD: Human mesenchymal stromal cells broadly modulate high glucose-induced inflammatory responses of renal proximal tubular cell monolayers. Stem Cell Res Ther 2019;10:1-19.
60 Wu MJ, Lai LW, Lien YH: Effect of calbindin-D28K on cyclosporine toxicity in cultured renal proximal tubular cells. J Cell Physiol 2004;200:395-399.
61 Thongboonkerd V, Zheng S, McLeish KR, Epstein PN, Klein JB: Proteomic identification and immunolocalization of increased renal calbindin-D28k expression in OVE26 diabetic mice. Rev Diabet Stud 2005;2:19-26.
62 Schwaller B: Cytosolic Ca2+ buffers. Cold Spring Harb Perspect Biol 2010;2:a004051.
63 Megyesi J, Andrade L, Vieira JM Jr, Safirstein RL, Price PM: Positive effect of the induction of p21WAF1/CIP1 on the course of ischemic acute renal failure. Kidney Int 2001;60:2164-2172.
64 Iwakura T, Fujigaki Y, Fujikura T, Ohashi N, Kato A, Yasuda H: Acquired resistance to rechallenge injury after acute kidney injury in rats is associated with cell cycle arrest in proximal tubule cells. Am J Physiol Renal Physiol 2016;310:F872-F884.
65 Price PM, Yu F, Kaldis P, Aleem E, Nowak G, Safirstein RL, Megyesi J: Dependence of cisplatin-induced cell death *in vitro* and *in vivo* on cyclin-dependent kinase 2. J Am Soc Nephrol 2006;17:2434-2442.
66 Grgic I, Campanholle G, Bijol V, Wang C, Sabbisetti VS, Ichimura T, Humphreys BD, Bonventre JV: Targeted proximal tubule injury triggers interstitial fibrosis and glomerulosclerosis. Kidney Int 2012;82:172-183.
67 Chevalier RL: The proximal tubule is the primary target of injury and progression of kidney disease: role of the glomerulotubular junction. Am J Physiol Renal Physiol 2016;311:F145-F161.